Supplementary information

High-rate mass transfer in a mesoporous catalyst with atomically dispersed cobalt sites enables efficient electrochemical synthesis of glycine

Xiaoxia Yu, Ke Chang, Juan Peng*

College of Chemistry and Chemical Engineering, Ningxia University, Yinchuan 750021, P. R. China.

* Corresponding author.
E-mail address: pengjuan@nxu.edu.cn

1 Experimental Section

1.1 Chemicals

Cobalt (II) acetate tetrahydrate, magnesium hydroxide, 1,10-phenanthroline monohydrate, glyoxylic acid, hydroxylamine, sodium nitrate, anhydrous ethanol, ammonium chloride, sulfuric acid, potassium sulfate, nitric acid were supplied by Sinopharm Chemical Reagent Co., Ltd. (Guoyao Reagent). Tert-butyl alcohol was obtained from Shanghai Macklin Biochemical Co., Ltd. Nessler's reagent, potassium sodium tartrate solution were supplied by Tianjin Jizhun Chemical Reagent Co., Ltd. N-(1-naphthyl) ethylenediamine dlhydrochlorlde, 3-aminobenzenesulfonamide, phosphoric acid, sodium acetate anhydrous, glacial acetic acid, ammonium iron(III) sulfate dodecahydrate, pyruvic acid, 2-oxobutanoic acid, 4-methyl-2-oxopentanoic acid, maleic acid were obtained from Shanghai Aladdin Biochemical Technology Co., Ltd. The Nafion solution (5 wt%) was supplied by Suzhou Sheng'erno technology Co., Ltd. All reagents are of analytical grade, and used as received without further treatment.

1.2 Characterizations

The XRD analysis was performed on a Japanese Smart Lab instrument with a scanning rate of 10°/min. The material's morphology was characterized using field-emission scanning electron microscopy (FE-SEM, ZEISS Sigma 560) and transmission electron microscopy (JEM-F200(URP)). Elemental characterization was carried out by energy-dispersive X-ray spectroscopy (EDXS) mapping on a JEOL ARM 200F instrument, while high-angle annular dark-field scanning transmission electron microscopy (HAADF-STEM) images were acquired to reveal atomic number (Z)-contrast and thickness variations. For atomic-resolution imaging, an aberration-corrected electron probe was operated at 200 kV. Nitrogen adsorption-desorption isotherms of the sample were measured at 77 K using a BSD-MAB multicomponent adsorption breakthrough analyzer, the specific surface area was obtained from the adsorption data by applying the Brunauer-Emmett-Teller (BET) model.The surface composition and chemical bonding states of the sample were analyzed by X-ray photoelectron spectroscopy (XPS, AXIS SUPRA+). Raman spectra were recorded on an XploRA Plus spectrometer. The metal Co content was determined by inductively coupled plasma optical emission spectrometry (ICP-OES) using an Agilent 5900 system.

Co K-edge X-ray absorption fine structure (XAFS) analyses were performed at the BL14W beamline of the Shanghai Synchrotron Radiation Facility (SSRF) (Shanghai, China) using a Si (111) crystal monochromator. The XAFS spectra were recorded at room temperature using a Bruker 5040 4-channel Silicon Drift Detector (SDD). The extended X-ray absorption fine structure (EXAFS) spectra at the Co K-edge were collected in transmission mode. The spectra were processed and analyzed using the Athena software package.

1.3 Electrochemical testing

Electrochemical measurements were carried out using an H-type electrochemical cell separated by a Nafion N-117 membrane between the cathode and anode compartments, coupled with a CHI 760E electrochemical workstation. The counter electrode and reference electrode were a Pt mesh and a Hg/Hg_2SO_4 electrode, respectively. The working electrode was prepared by dispersing the as-prepared catalyst (5 mg) in a mixed solution of deionized water and ethanol (1:1, v/v, 500 μL), and adding Nafion solution (5 wt %, 25 μL), followed by ultrasonic dispersion for 1 h, then casting onto

a conductive carbon substrate (TGP-H-060) with a catalyst loading of 1 mg cm^{-2}. The anolyte was an aqueous H_2SO_4 solution, and the catholyte varied according to the reaction requirements, the specific compositions are detailed in the respective sections of the original manuscript.

Linear sweep voltammetry (LSV) curves were recorded at a scan rate of 50 mV s^{-1}. When adjusting the proton and substrate concentrations of the electrolyte, chronoamperometric experiments were conducted at a constant potential of -0.85 V vs RHE for 3 h. During the electrosynthesis of glycine, chronoamperometric measurements were performed at different potentials for 3 h. Prior to all 3 h chronoamperometric experiments, Ar was bubbled through the catholyte for 20 min.

According to the *equation*:

$E_{RHE} = E_{Hg/Hg2SO4} + 0.0592 \times PH + 0.658V$

all potentials were converted to the reversible hydrogen electrode.

1.4 Identification and quantification of products

After electrolysis, gaseous products were analyzed by a Tianmei GC-7900 gas chromatograph. Liquid products (glycine, glyoxylic acid (GX), glycolic acid (GC), oxime) were qualitatively and quantitatively determined by ^1H NMR spectroscopy using a Bruker Avance III 500 MHz spectrometer. For sample preparation, 400 μL of electrolyte was mixed with 100 μL of dimethyl sulfoxide (DMSO, 28.16 mM) and 100 μL of D_2O, and the resulting mixture was used directly for NMR analysis. The concentrations of NO_2^-, NH_2OH, and NH_4^+ were measured by UV–Vis spectrophotometry, the procedures for determining NO_2^-, NH_4^+, and NH_2OH by UV–Vis spectrophotometer are discussed below.

Quantitative analysis process of NO_2^-. A colour reagent was prepared by dissolving 2.00 g of 3-aminobenzenesulfonamide, 0.10 g of N-(1-naphthyl) ethylenediamine dlhydrochlorlde, and 5 mL of concentrated phosphoric acid in deionized water, and diluting to a final volume of 50 mL. After completion of the reaction, 5 mL of electrolyte was mixed with 1 mL of the freshly prepared colour reagent, and the mixture was diluted to 50 mL with deionized water. The resulting solution was allowed to stand at room temperature for 20 min prior to UV-Vis spectroscopic analysis. A series of standard solutions with known concentrations of NO_2^- was prepared, and the absorbance at 540 nm was measured to construct a calibration curve (Fig. S1) for quantitative determination.

Quantitative analysis process of NH_2OH. Based on the reduction of Fe^{3+} to Fe^{2+} by NH_2OH, Fe^{2+} can form an orange complex with 1,10-phenanthroline for the quantification of NH_2OH. A certain amount of sample was sequentially mixed with 1 mL of acetate buffer aqueous solution (composed of 1 M sodium acetate and 1 M glacial acetic acid), 1 mL of 4 mM ammonium iron(III) sulfate dodecahydrate (0.1 M nitric acid as solvent), and 1 mL of 10 mM 1,10-phenanthroline ethanol solution. Then the mixture was diluted to 50 mL with deionized water and allowed to stand at room temperature for 20 min, followed by UV-Vis spectral analysis. Using standard solutions with known NH_2OH concentrations, a calibration curve (Fig. S2) was generated based on the maximum absorbance at 510 nm.

Quantitative analysis process of NH_4^+. A certain amount of sample was taken and diluted with deionized water to 45 mL, and then sequentially mixed with 1 mL of potassium sodium tartrate solution and 1 mL of Nessler's reagent, followed by dilution to 50 mL with deionized water. The mixture was allowed to stand at room temperature for 20 min, and UV-Vis spectral analysis was performed. Using standard solutions with known ammonium chloride concentrations, a calibration

curve (Fig. S3) was generated based on the maximum absorbance at 420 nm.

1.5 Calculation of key parameters

Faraday efficiency (FE) of liquid products was calculated using the following *equation*:

$$FE(\%) = \frac{N \times F \times C \times V}{Q} \times 100\%$$

where C is the concentration of the product formed after electrolysis. N is the number of electrons transferred per mole of product. V represents the volume of the catholyte. F is the Faraday constant (96485 C mol^{-1}). Q is the total charge passed during the electrochemical reaction.

Concentration (c) of products in catholyte were calculated based on the following *equation*:

$$C = \frac{6 \times V_0 \times S \times C_0}{n \times V \times S_0}$$

where V_0 is the volume of the DMSO solution used in the ^{1}H NMR measurement (100 μL), C_0 is the concentration of the DMSO solution (28.16 mM), 6 represents the number of equivalent hydrogen atoms of DMSO in the ^{1}H NMR spectrum, S_0 is the peak area of DMSO in the ^{1}H NMR spectrum, V is the volume of the catholyte used in the ^{1}H NMR measurement (400 μL), C is the concentration of the product, n represents the number of equivalent hydrogen atoms of the product giving rise to the ^{1}H NMR signal, and S is the peak area of the product in the ^{1}H NMR spectrum.

The calculation of glycine selectivity:

$$Glycine\ selectivity = \frac{n_{Glycine}}{n_{Glycine} + n_{GX} + n_{GC} + n_{GAO}} \times 100\%$$

where n represents the amount of substance of each product after electrolysis for 3 h.

The calculation of GX conversion rate:

$$Conversion(\%) = \frac{C_0 - C_t}{C_0} \times 100\%$$

where C_0 and C_t represent the concentrations of GX at the initial time and at time t, respectively.

The calculation of glycine yield rate:

$$Production\ rate(\mu mol\ h^{-1}\ cm^{-2}) = \frac{n_{Glycine}}{t \times A}$$

where $n_{Glycine}$ is the amount of glycine determined by ^{1}H NMR (in micromoles). t is the reaction time (hours). A is the geometric area of the carbon fiber paper (1 cm^{-2}).

1.6 In situ ATR-FTIR measurements

The in situ ATR-FTIR measurements were performed on a Thermo Scientific Nicolet 6700 spectrometer equipped with a liquid-nitrogen-cooled mercury cadmium telluride (HgCdTe) detector. The electrode system was assembled on an ATR liquid cell, and the in situ electrochemical tests were conducted using a CHI 760E electrochemical workstation. The working electrode was pressed against the ZnSe crystal window to minimize infrared loss. An Ag/AgCl electrode (saturated with KCl solution) and a platinum wire were used as the reference electrode and counter electrode, respectively. Spectra were acquired in reflection mode with vertical incidence of the infrared beam to ensure spectral quality. Before the reaction, background spectra of the electrocatalyst were collected at the open-circuit potential. For the reaction, chronoamperometry was used, and the spectra were recorded simultaneously (32 scans at a resolution of 4 cm^{-1}).

2 Supplementary Figures and Tables

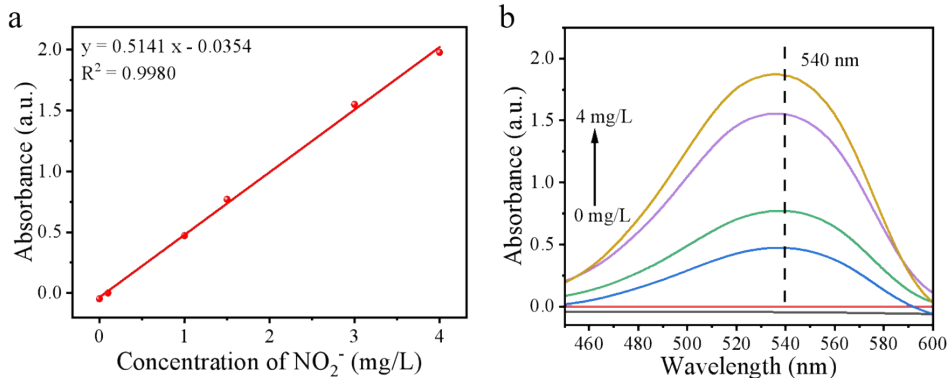

Fig. S1 (a) Estimated calibration curve at 0-4 mg L^{-1} of NO_2^-, and (b) UV-vis spectra.

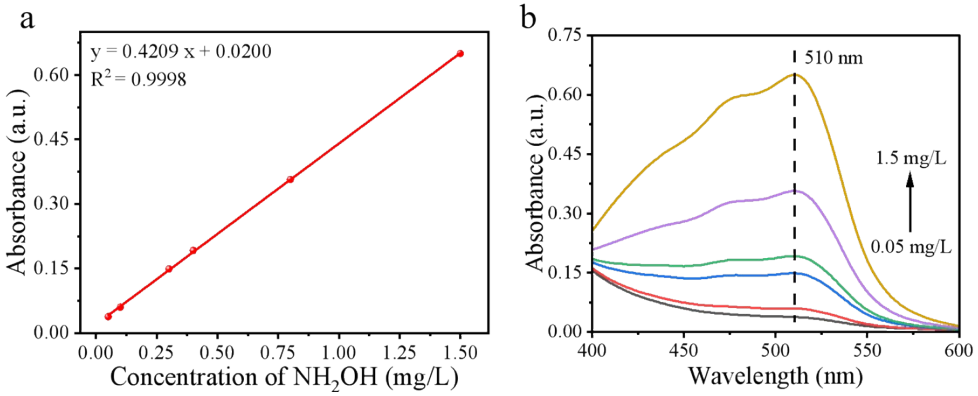

Fig. S2 (a) Estimated calibration curve at 0.05-1.5 mg L^{-1} of NH_2OH, and (b) UV-vis spectra.

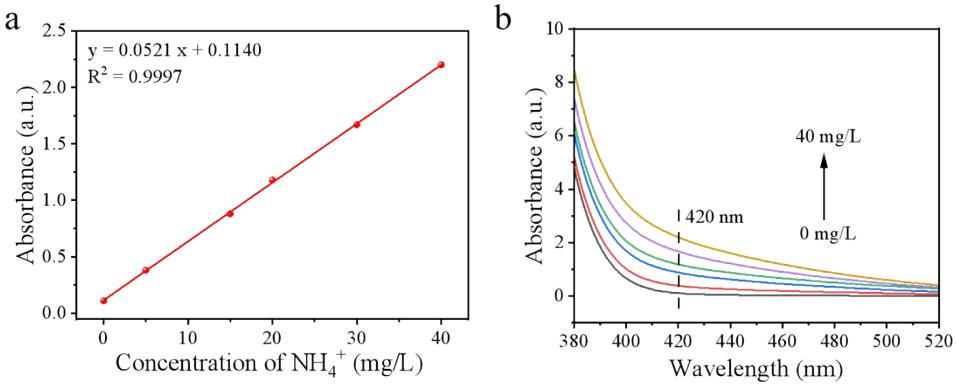

Fig. S3 (a) Estimated calibration curve at 0-40 mg L^{-1} of NH_4^+, and (b) UV-vis spectra.

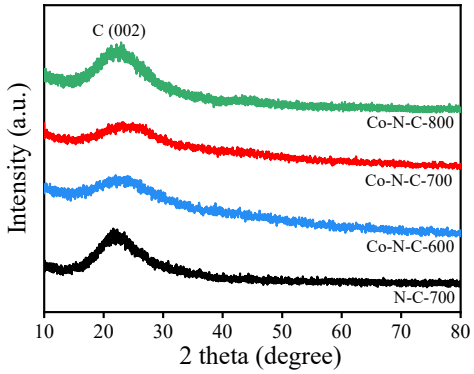

Fig. S4 The XRD patterns of N-C-700, Co-N-C-600, Co-N-C-700, Co-N-C-800.

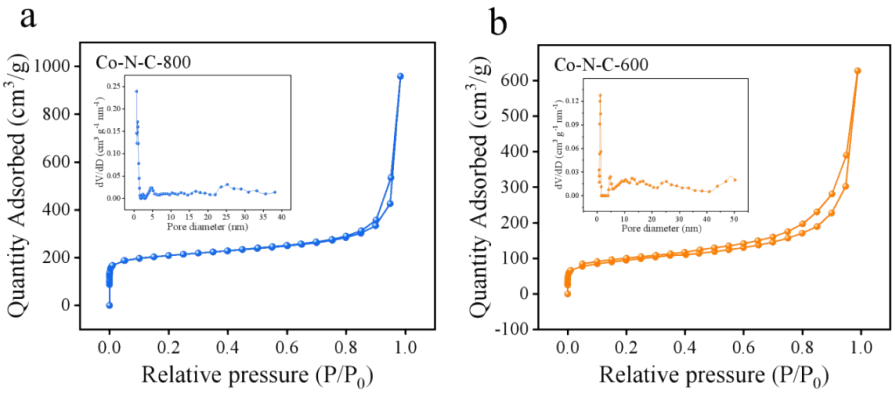

Fig. S5 N_2 adsorption-desorption isotherms of Co-N-C-800 (a), and Co-N-C-600 (b), the inset shows the pore size distribution.

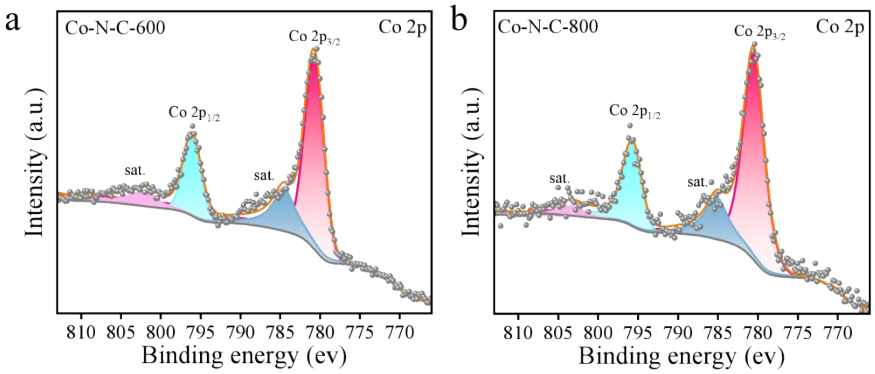

Fig. S6 Co 2p XPS spectrum of Co-N-C-600 (a), and Co-N-C-800 (b).

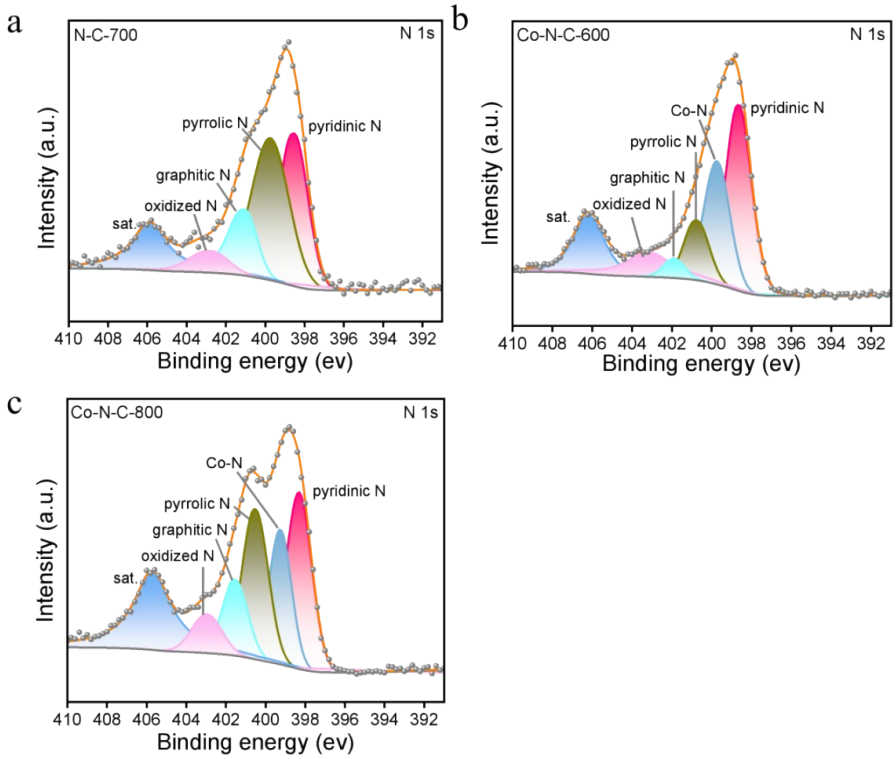

Fig. S7 High-resolution XPS of N 1s regions (a) N-C-700, (b) Co-N-C-600, (c) Co-N-C-800.

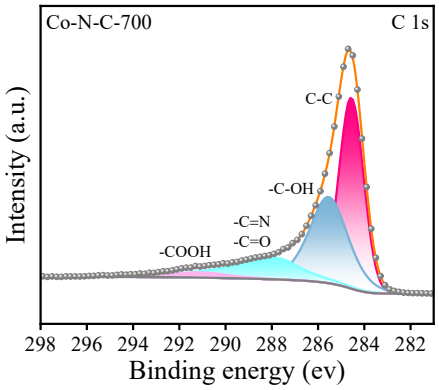

Fig. S8 C 1s XPS spectrum of Co-N-C-700.

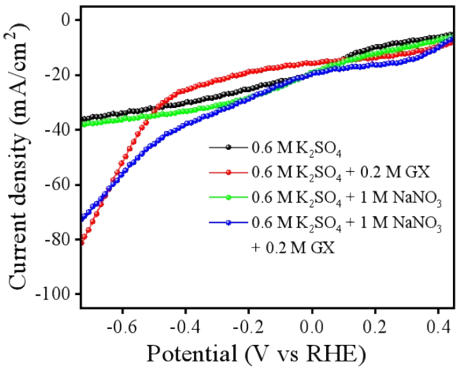

Fig. S9 LSV curves in different electrolyte for Co-N-C-700 .

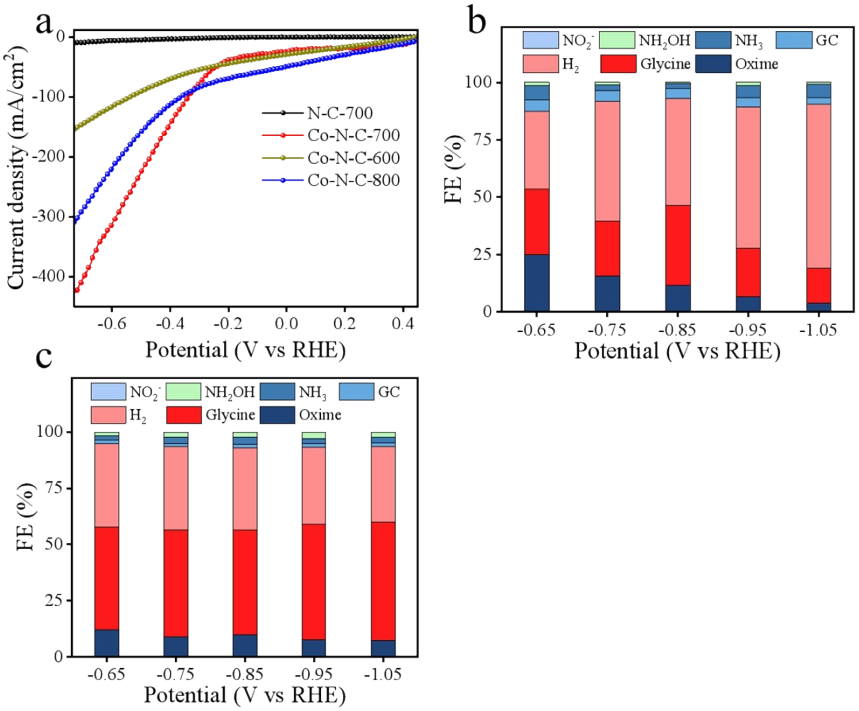

Fig. S10 (a) LSV curves, product distribution at different applied potentials for (b) Co-N-C-600 and (c) Co-N-C-800 in an electrolyte containing 1 M NO_3^-, 0.2 M GX, and 0.6 M H_2SO_4.

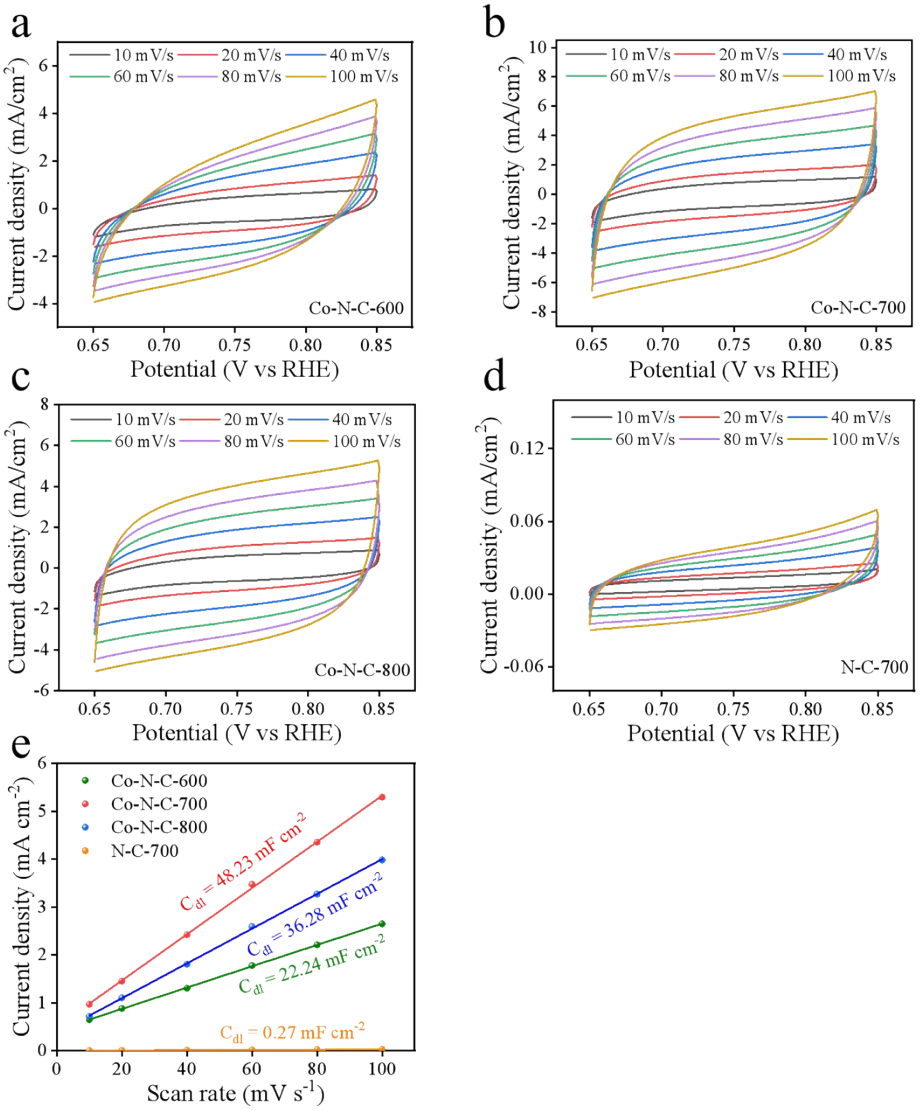

Fig. S11 CV curves of (a) Co-N-C-600, (b) Co-N-C-700, (c) Co-N-C-800, (d) N-C-700 under different scanning speeds (10-100 mV s^{-1}). (e) Linear fitting of the average variance of anode current and cathode current at different scan rates at 0.75 V vs RHE. Electrolyte: 0.6 M H_2SO_4; 0.2 M GX; 1.0 M $NaNO_3$.

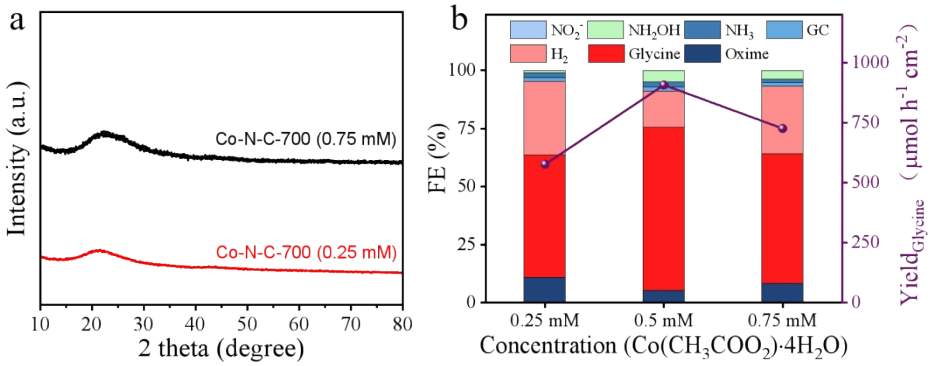

Fig. S12 (a) The XRD patterns of Co-N-C-700 (0.25 mM), and Co-N-C-700 (0.75 mM). (b) Product distribution, and glycine yield obtained with different cobalt precursor loadings.

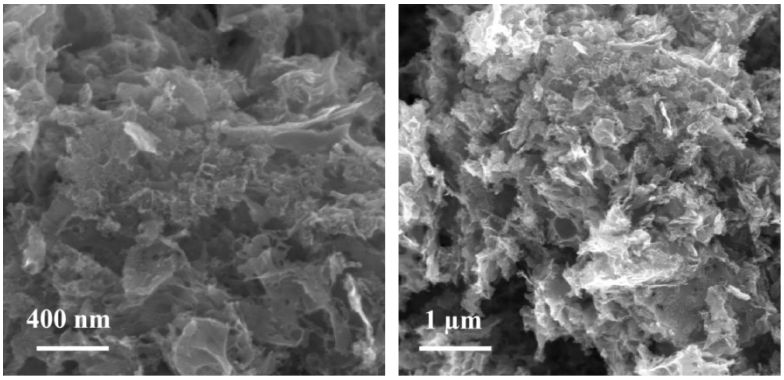

Fig. S13 SEM image of Co-N-C-700 after 15 electrolysis cycles.

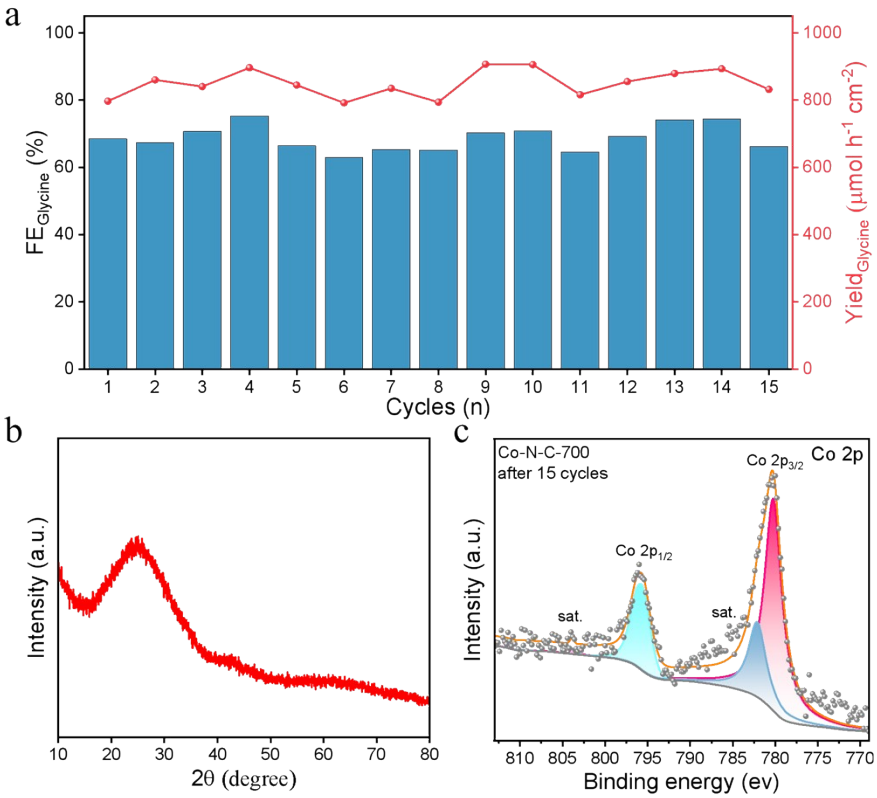

Fig. S14 (a) Cycling stability test of Co-N-C-700 at -0.85 V vs RHE, 1 M NO_3^-, 0.2 M GX, and 0.6 M H_2SO_4. (b) XRD pattern and (c) XPS spectrum of Co-N-C-700 after 15 electrolysis cycles.

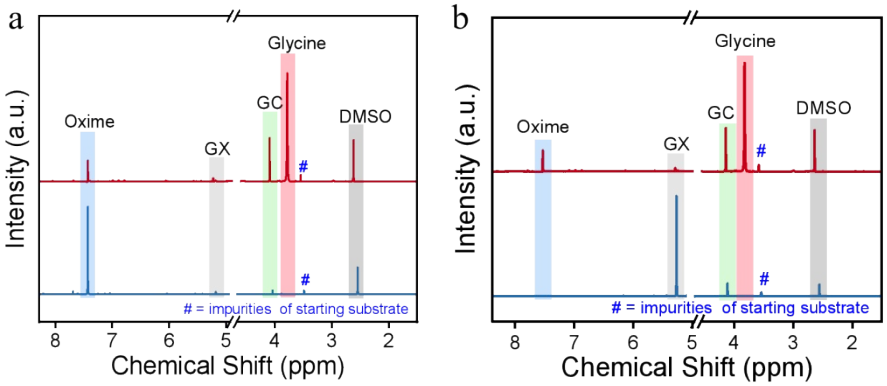

Fig. S15 (a) The ^{1}H NMR spectrum of oxime standard (blue), and ^{1}H NMR spectrum of distribution of electrolysis products at -0.85 V vs RHE, 1 M NO_3^-, 0.2 M GX, and 0.6 M H_2SO_4

(red). (b) The ^{1}H NMR spectrum of distribution of electrolysis products at -0.85 V vs RHE, 0.2 M GX, and 0.6 M H_2SO_4 (blue).

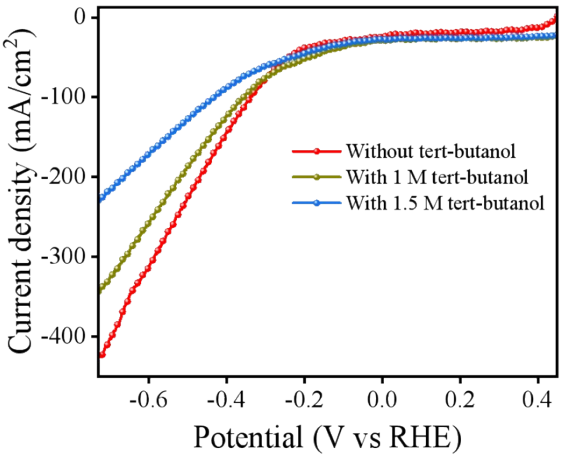

Fig. S16 LSV curves measured with the addition of tert-butanol as a *H scavenger in an electrolyte containing 0.2 M GX, 1 M $NaNO_3$, and 0.6 M H_2SO_4.

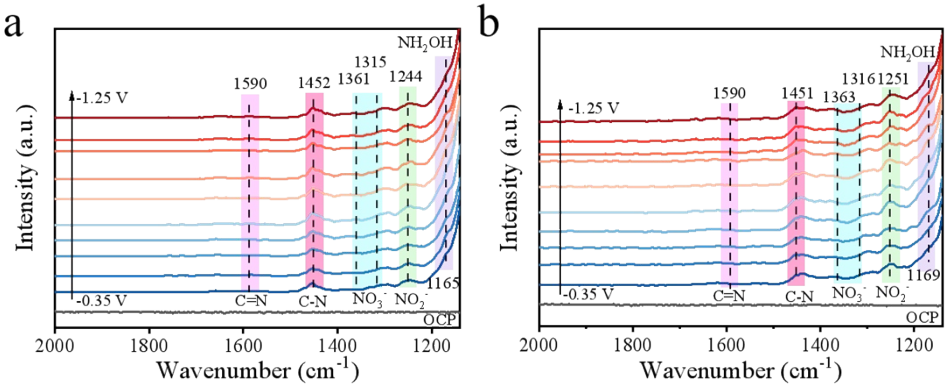

Fig. S17 In-situ ATR-FTIR spectra recorded during the co-reduction of GX and NO_3^- over Co-N-C-800 (a), and Co-N-C-600 (b).

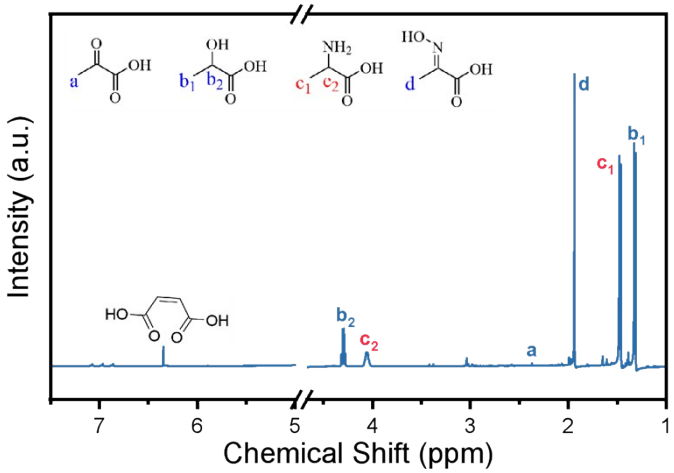

Fig. S18 ^{1}H-NMR spectrum of electrolyte by using Co-N-C-700 electrode after 3h in electrocatalytic synthesis of alanine at -0.85 V vs RHE.

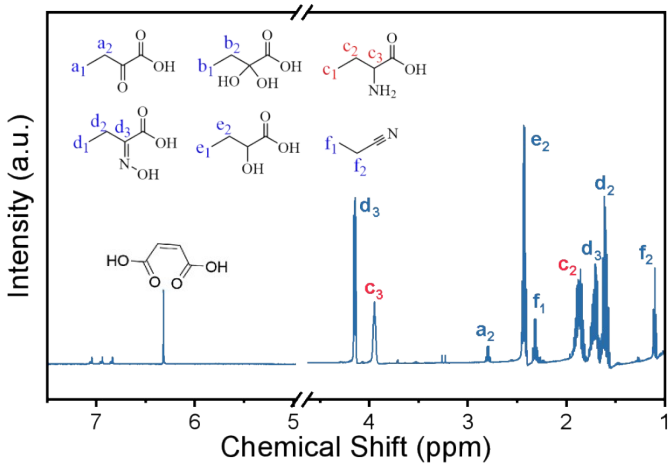

Fig. S19 ^{1}H-NMR spectrum of electrolyte by using Co-N-C-700 electrode after 3h in electrocatalytic synthesis of 2-aminobutyric acid at -0.85 V vs RHE.

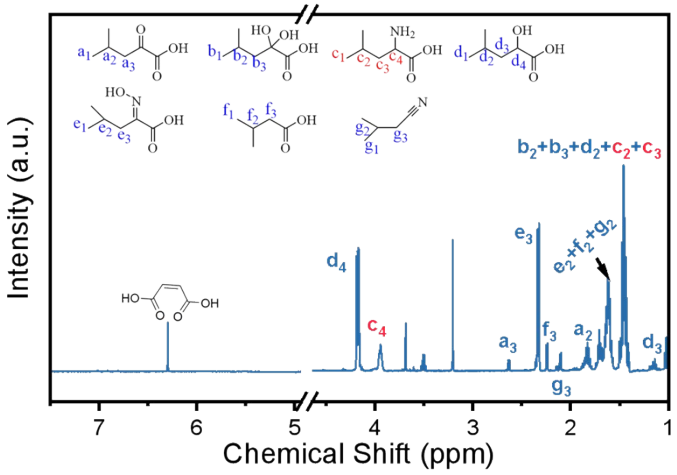

Fig. S20 ^{1}H-NMR spectrum of electrolyte by using Co-N-C-700 electrode after 3h in electrocatalytic synthesis of leucine at -0.85 V vs RHE.

Table S1 Brunauer-Emmett-Teller measurement summary reports of Co-N-C-600, Co-N-C-700, and Co-N-C-800.

Catalysts	S_{BET} ($m^2\ g^{-1}$)	S_{Micro} ($m^2\ g^{-1}$)	S_{Meso} ($m^2\ g^{-1}$)	V_{Pore} ($cm^3\ g^{-1}$)	S_{Micro}/S_{BET} (%)	S_{Meso}/S_{BET} (%)
Co-N-C-700	546.82	357.25	189.57	0.69	65.33	34.67
Co-N-C-800	782.30	595.58	186.72	0.76	76.13	23.87
Co-N-C-600	335.40	151.46	183.94	0.71	45.16	54.84

Table S2 Fitting results of EXAFS spectra.

Sample	Scattering path	N	R (Å)	σ^2 ($Å^2$)	ΔE_0 (eV)	R factor (%)
Co-N-C-700	Co-N	3.95±0.34	2.06±0.03	0.011	-2.72±0.90	0.0094

N: coordination number; R: bond distance; σ^2: Debye-Waller factor; ΔE_0: the inner potential correction. R factor: goodness of fit. S_0^2 was fixed as 1.0. Date range: $3 < k < 12$ $Å^{-1}$, $1 < R < 3$ Å. The number of variable parameters is 4, out of a total of 10.18 independent date points.

Table S3 Performance comparison of electrochemical synthesis of glycine.

Catalyst	C_{source}	N_{source}	Operating potentials V (vs RHE)	Conversion (%)	Selectivity (%)	Production rate ($\mu mol\ h^{-1}\ cm^{-2}$)	FE (%)	Reference
Co-N-C-700	**GX**	**NO_3^-**	**-0.85**	**100**	**79.03**	**907.1**	**70.3**	**This work**
$_{ad}$Fe-TiO_x/Ti	GX	NO_3^-	-0.7	100	80.2	236.1	31.0	[1]
Co-HCNF	GX	NO_3^-	---	---	---	159.5	42.8	[2]
ed-PbCu	OA	NH_2OH	---	---	---	---	78.8	[3]
$CuPb_{1ML}$	OA	NH_2OH	-1.3	76.0	63.2	211	57.0	[4]
CuSn	GX	NO_3^-	-0.2	100	99.32	39.83	78.7	[5]
Cu/Bi-C@CF	GX	NO_3^-	---	100	89	198.48	65.9	[6]
WOx/D-CB	GX	NO_3^-	-0.5	---	---	93.00	49.3	[7]
CoPc/CNT	GX	NO_3^-	-0.57	---	---	---	47.0	[8]
CoFe-SSM	GX	NO_3^-	-0.7	---	---	164.41	41.2	[9]
Pb/Pb_7Bi_3	OA	NO_3^-	-1.0	---	---	172.9	91.8	[10]
Cu-Hg	GX	NO_3^-	-1.0	---	---	31.0	43.1	[11]

References

1 Z. Zhu, Y. Jiang, L. Xu, Q. An, T. T. T. Nga, J. Chen, Y. Fan, Q. Liu, C. L. Dong, S. Wang and Y. Zou, Highly efficient synthesis of α-amino acids via electrocatalytic C-N coupling reaction over an atomically dispersed iron loaded defective TiO_2, Adv. Mater., 2025, **37**(5), 2409864.

2 J. Xian, K. Cai, P. Liao, S. Wang and G. Li, Upgrading waste NO_x into amino acids via electrocatalysis on Co nanoparticles encapsulated in hollow carbon nanofibers, Sci. China Chem., 2024, **67**(6), 1946-1952.

3 L. Li, C. Wan, S. Wang, X. Li, Y. Sun and Y. Xie, Tandem dual-site PbCu electrocatalyst for high-rate and selective glycine synthesis at industrial current densities, Nano Lett., 2024, **24**(7), 2392-2399.

4 P. J. Broersen, T. de. Groot, D. F. Bruggeman, E. S. Caarls, J. A. Trindell, D. Anastasiadou, M. C. Figueiredo, G. Rothenberg and A. C. Garcia, Enhancing electrocatalytic synthesis of glycine with $CuPb_{1ML}$ electrode synthesized via Pb UPD, ChemCatChem, 2024, **16**(4), e202301370.

5 W. Zhou, Y. Wu, W. Zhang, Z. Chen, Z. Gao, J. Li, K. Yu, Y. B. He, B. Liu and F. Kang, Highly selective electrosynthesis of glycine from glyoxylic acid and nitrate via stabilizing the NH_2OH intermediates, Angew. Chem. Int. Ed., 2026, **65**(3), e16749.

6 P. Liao, B. Zeng, S. Li, Y. Zhang, R. Xiang, J. Kang, Q. Liu and G. Li, Cu-Bi bimetallic catalysts derived from metal-organic framework arrays on copper foam for efficient glycine electrosynthesis, Angew. Chem. Int. Ed., 2025, **64**(5), e202417130.

7 G. Wu, Z. Ma, T. Heil, L. Zhang, W. Hu, G. Wu, W. He, L. Dai, Y. Huang and Q. Qin, Boosting amino acid synthesis with WO_x sub-nanoclusters, Adv. Mater., 2025, **37**(9), 2418233.

8 Y. Zhou, R. Duan, Q. Huang, C. Ding and C. Li, Amino acid synthesis through C-N coupling between α-ketoacids and hydroxylamine from nitrate reduction, ACS Catal., 2024, **14**(13), 10164-10171.

9 J. Xian, S. Li, H. Su, P. Liao, S. Wang, R. Xiang, Y. Zhang, Q. Liu and G. Li, Electrosynthesis of α-amino acids from NO and other NO_x species over CoFe alloy-decorated self-standing carbon fiber membranes, Angew. Chem. Int. Ed., 2023, **135**(30), e202306726.

10 P. Li, Y. Wang, X. Zhang, C. Wang, Y. Hou, G. Zhang, X. Wang, L. Jing, Q. Qian and X. Kang, Efficient glycine electrosynthesis via CO_2-recyclable hydrogen donation on Pb/Pb_7Bi_3 heterointerfaces, Angew. Chem. Int. Ed., 2025, **137**(40), e202514321.

11 J. E. Kim, J. H. Jang, K. M. Lee, M. Balamurugan, Y. I. Jo, M. Y. Lee, S. Choi, S. W. Im and K. T. Nam, Electrochemical synthesis of glycine from oxalic acid and nitrate, Angew. Chem. Int. Ed., 2021, **133**(40), 22114-22122.